

# **PRESSURE DROP AND TEMPERATURE DROP ANALYSIS OF THE OPTIMAL TOP CAP DESIGN OF EVAPORATOR OF THE MICRO LOOP HEAT PIPE**

**Praveen K. Arragattu, Frank M. Gerner**

Department of Mechanical, Industrial and Nuclear Engineering,  
University of Cincinnati,  
Cincinnati, Ohio 45221-0030.

**H. T. Henderson**

Department of Electrical and Computer Engineering and Computer Science,  
University of Cincinnati,  
Cincinnati, Ohio 45221-0030.

## **ABSTRACT**

The Micro Loop Heat Pipe (LHP) is a revolutionary device that may be used to cool microelectronics, solar collectors and other devices in microgravity applications. It is a two phase cooling device with extremely high effective thermal conductivity that utilizes the capillary forces developed inside its wicked evaporator and the thermodynamic pressure difference developed between the evaporator and the condenser to circulate a working fluid through a closed loop. The most important part of the loop heat pipe is the evaporator. It consists of top cap, coherent silicon porous (CPS) wick and the compensation chamber. Very few studies and experiments have been performed in determining the efficient and optimal design of the top cap. The main problem with the top caps designed in the past was associated with the conduction of heat from the source to the primary wick and this problem reduced the heat dissipation ability of the loop heat pipe. Five new optimal top cap designs were studied to overcome this problem with the provision of conduction pathways. Each of the five designs is briefly discussed. The conditions used for arriving at the optimal solutions were discussed. Calculation of pressure drop and temperature drop was very essential for the determination of optimal solutions of the top cap. For the trapezoidal slot and trapezoidal mesas top cap design the pressure drop and temperature drop calculations were discussed in detail. Geometry of the external vapor reservoir for the trapezoidal slot top cap was designed for optimum pressure drop. Variation of pressure drop in the top cap with respect to the porosity in the coherent porous silicon wick is discussed and analyzed in detail. The exact pressure drop calculations were performed numerically using a finite volume commercial flow solver FLUENT 6.1 with appropriate boundary conditions. The temperature drop calculations were performed using finite element modeling in ANSYS 6.1. It was assumed that all the pores have uniform mass flow rate and were at saturation conditions during the phase change.

## **INTRODUCTION**

Packing more transistors onto a chip and microprocessors into the computer system resulted in increase of the computing power. But it exponentially increased the power densities generating high concentrated heat near the heat source which has to be removed before the material melted. Reliability issues, additional power needs, increasing operational costs and adverse environmental impacts avoid the use of refrigeration systems for electronics cooling. Cooling of microprocessors and micro-electronic chip modules (MCM) was made possible by forced convection. Recently the

phase change devices are used in cooling of electronics and MCM's. Space applications requiring cooling micro-electronic devices, solar power collectors require lightweight cooling equipment which reduces the launching cost and diminishes cost of maintenance. Therefore, NASA is highly interested in the phase change devices like micro loop heat pipes where no pump is needed.

The Micro Loop Heat Pipe (LHP) is a revolutionary two phase cooling device which uses the capillary forces generated inside its pores to transport the heat from the higher temperature source to the low temperature sink. The condensed liquid flows back into the compensation chamber which acts as a reservoir for maintaining the sufficient amount of working fluid in the system as shown in the Fig.1 (a), (b).

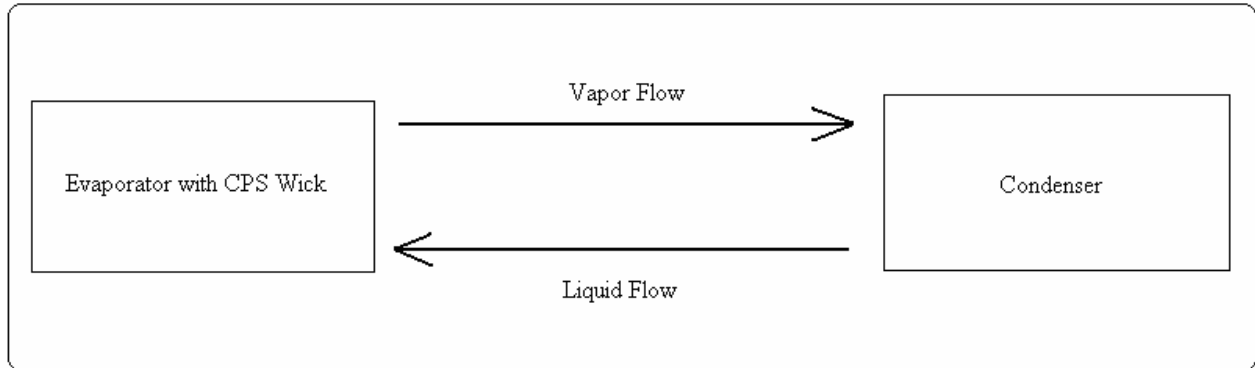


Figure 1: (a) Schematic of the Loop Heat Pipe.

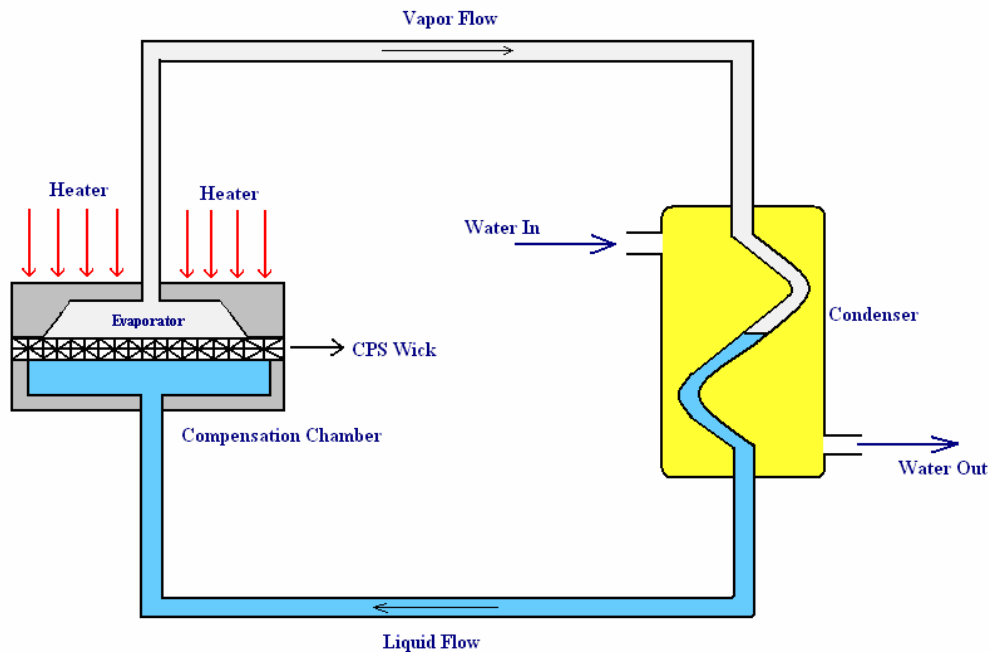


Figure 1: (b) Basic Loop Heat Pipe.

The loop heat pipe is a passive device without any moving parts that utilizes the thermodynamic pressure difference developed between the evaporator and condenser and the capillary forces developed inside its wicked evaporator to circulate a working fluid through a closed loop. The liquid medium present in the LHP is converted into the vapor on absorption of heat from the source.

Generated vapor pressure inside the evaporator circulates the mass around the loop. The maximum value of this vapor pressure should not exceed the capillary pressure of the wick. Vapor flows from evaporator to the condenser because of the thermodynamic pressure difference between the two. Vapor is condensed to liquid in the condenser after losing its latent heat. The condensed liquid flows back into the compensation chamber which acts as a reservoir for maintaining the sufficient amount of working fluid in the system. The working fluid is pumped into the primary wick where evaporation occurs through the secondary wick present in the compensation chamber. Commercially available Loop Heat Pipes are based on annular cylindrical sintered ceramic or metallic wick structure. Distribution of pore sizes are not uniform in the sintered wick structure and burst through pressure is low as it is dominated by largest pore in the wick. On the other hand, Micro LHP developed by utilization of MEMS technology has number of discerning characteristics. Its planar shape in contrast to the cylindrical shape enables it to cool most of the desired surfaces. The primary wick in the evaporator package is made of silicon making the integration of microelectronics easier. More uniform pores of sub micron size can be realized in the wick using MEMS based fabrication techniques resulting in high burst through pressures.

The basic components of the loop heat pipe are evaporator, vapor line, condenser, liquid line and compensation chamber as shown in Fig. 1 (b). The most important part of the loop heat pipe is the evaporator. It consists of top cap, coherent silicon porous wick and the compensation chamber. Very few studies and experiments have been performed in determining the efficient and optimal design of the evaporator top cap. Alexseev [1] determined the optimal geometric parameters of the evaporator top cap based on the maximum evaporation rate of the single pore. Alexseev basically assumed that there was no heat leak to the compensation chamber. Mohammad et al [2] and Holke et al [3] worked on the diameter optimization of the coherent silicon porous wick. A piecewise model was used by Mohammad [2] to describe the whole loop including the five major elements in the loop heat pipe, which are wicked evaporator, compensation chamber, condenser, vapor line and liquid line. Mohammad et al [2] presented a steady state model of the loop heat pipe by arriving and solving a set of seven closure equations. Also Holke et al [3] showed that an effective way to increase the loop heat pipe performance is by reducing the pressure drop in the evaporator. Chandratilleke et al [4] showed that loop heat pipe can work in a cryogenic temperature range of 4 K to 77K. Chandratilleke et al [4] investigated four different working fluids to develop a loop heat pipe that could transport at least 10 times the amount of heat as compared to a solid copper rod of the same size. The differences between the loop heat pipe and capillary pumped loop are discussed in detail by Nikitkin et al [5]. The major arrangement design difference between these two systems is the position of the compensation chamber. Swanson and Herdt [6] reported a theoretical model for meniscus evaporation including Marangoni effect as well as London-Van der Waal dispersion forces. The mathematical model of the steady state behavior of the loop heat pipe is presented by Kaya et al [7]. Interfacial oscillation related to loop heat pipe is presented by Kamotani et al [8]. According to Kamotani et al [8], the interfacial oscillation depends upon the critical temperature difference between the heater and the sidewall. Tarik et al [9] conducted the tests at varying heat load and condenser sink temperatures at different orientations of LHP. Tarik et al [9] successfully demonstrated the start up of the LHP at heat loads as low as 5 W. They observed that the small LHP could continue to operate for long time because of parasitic heating, even after applied power was removed. Numerical simulation of the flow in capillary pumped loop was studied by Figus et al [10] and found that capillary fingering may limit the performance of the loop. Thiago et al [11] presented a mathematical model that was able to predict the LHP operation temperature. They used acetone as the working fluid.

The main objective of the top cap of the evaporator of LHP is to conduct energy from the heat source to the menisci of the liquid- vapor interface inside the porous wick and to provide vapor

channels which helps in carrying the vapor away from the vapor side of the wick to the condenser. The main problem with the top caps designed in the past was associated with the conduction of heat from the source to the wick and this problem reduced the heat dissipation ability of the loop heat pipe. The objective of conducting the heat energy effectively from the source to the wick was achieved by providing conduction pathways. The top cap with and without the conduction pathways are as shown in the Fig. 2 below.

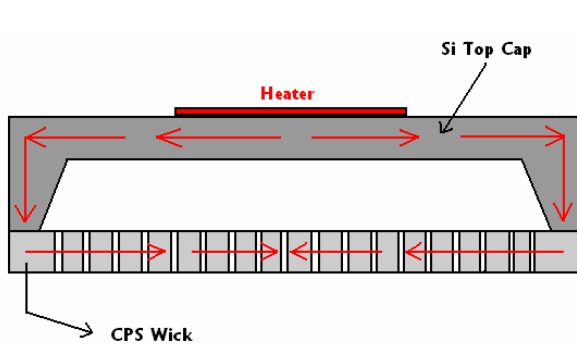


Figure 2: (a) Heat conduction in top cap over CPS wick without conduction pathways.

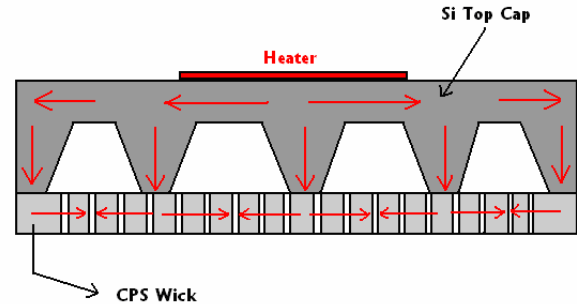


Figure 2: (b) Heat conduction in top cap over CPS wick with conduction pathways.

It can be seen from the Fig. 2 (a) that the heat is conducted to the CPS wick laterally from the sides of the silicon top cap leaving many of the pores in the center unheated. Finite element modeling showed very high temperature drop of approximately  $39^{\circ}\text{C}$  from the center of the top cap to the center of the wick for the heat input of 4 W. This resulted in the non-uniform heat and temperature distribution on the surface of the wick, which drastically affect the power dissipation capacity of the micro loop heat pipe. The heat energy was effectively conducted from the source to the wick by providing conduction pathways as shown in the Fig. 2 (b). The heat and temperature distribution was uniform on the wick with the provision of conduction pathways. The top cap with conduction pathways had high pressure drop compared to the top cap without conduction pathways due to increased velocity of the vapor flow with reduction in the vapor area. Optimal configuration of the conduction pathways was very essential as it increased the pressure drop and decreased the temperature drop. Five feasible competitive designs of the top cap with the conduction pathways from the fabrication point of view were identified and presented in the Fig. 3 shown below.

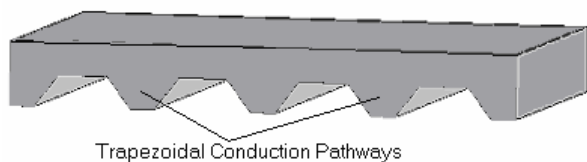


Figure 3: (a) Trapezoidal slot top cap design.

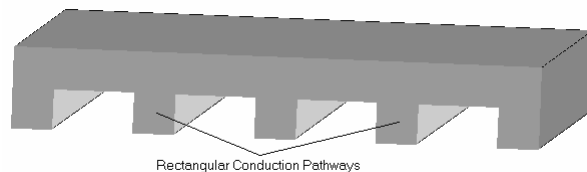


Figure 3: (b) Rectangular slot top cap design.

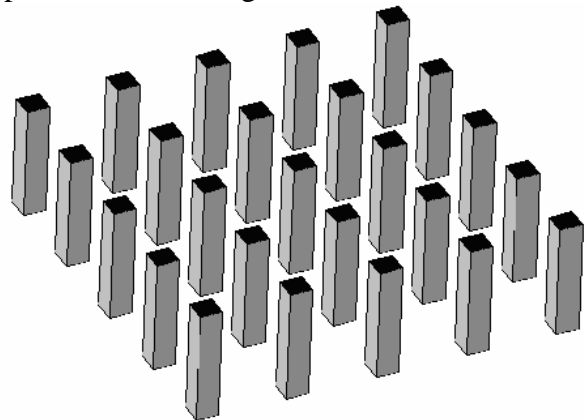


Figure 3: (c) Square columns top cap design.

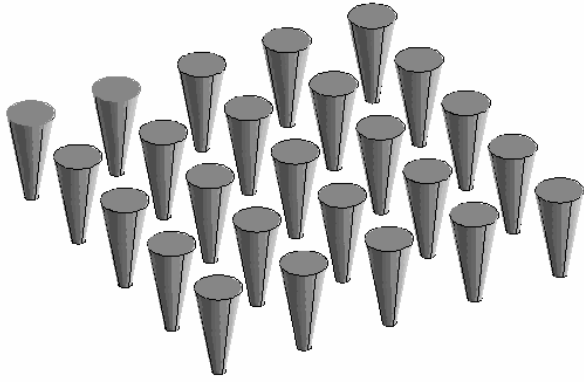


Figure 3: (d) Cone columns top cap design.

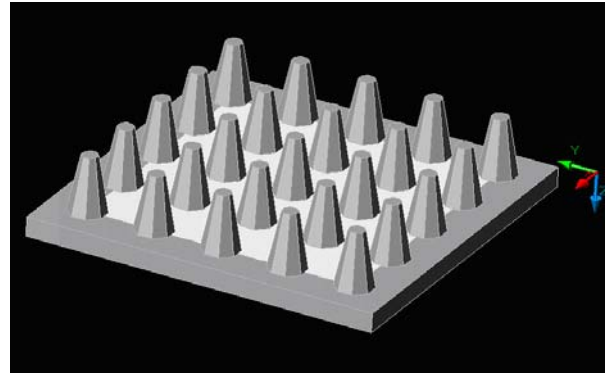


Figure 3: (e) Trapezoidal Mesas top cap design.

- Trapezoidal Slot Top Cap: This competitive top cap design can be fabricated on the Silicon  $\langle 100 \rangle$  plane. Angle of KOH etching in the above design model was found to be  $54.74^\circ$ .
- Rectangular Slot Top Cap: This competitive top cap design can be fabricated on the Silicon  $\langle 110 \rangle$  plane. Angle of KOH etching in the above design model was found to be  $90^\circ$ .

In the above two designs the vapor generated flows from the center of the channel to the reservoirs provided at both ends. There is an additional pressure drop due to these reservoirs.

Square Columns, Cone Columns and Trapezoidal Mesas can all be fabricated on the Silicon  $\langle 100 \rangle$  plane with different etching angles. The etching angle for the trapezoidal mesas was found to be  $70.7^\circ$ . In these top cap designs the vapor exits from the center of the top cap with only one outlet. Pressure drop and temperature drop calculation is very essential for the determination of optimal top cap geometry. Arragattu et al [12] presented an approximate model for the calculation of pressure drop for each of the design using a simple 2D microchannel principle.

Optimal solutions characterized by geometric parameters were done with the following constraints:

- Pressure Drop in the top cap is less than 2500 Pascal as the heat leak associated with this pressure drop is less. The burst through pressure was generally around 25000 Pa so the above pressure drop constraint was very less than this value.
- Temperature drop in the top cap is less than  $10^\circ$  C. The heat leak to the compensation chamber was very high if the temperature drop is more than  $10^\circ$  C.
- Number of pores covered by the conduction pathways on the wick is minimum to avoid maximum evaporation rate limit per pore.

Of the five designs, trapezoidal slot and trapezoidal mesas top cap were considered for fabrication as they were relatively easy to fabricate with the available MEMS fabrication technology. Geometries of the trapezoidal slot and trapezoidal mesas top cap were chosen from the optimal solutions for perfect contact shown in table [1] based on the approximate analysis of pressure and temperature drop given by Arragattu et al [12]. The geometry of the top cap was modeled in GAMBIT 2.1 and exact pressure drop was numerically calculated using a finite volume commercial flow solver FLUENT 6.1. Uniform velocity inlet boundary condition with no slip was used for all inlet faces. Gauge pressure outside the vapor exit was taken as zero. The temperature drop in the conduction pathways was determined by finite element modeling in ANSYS 6.1.



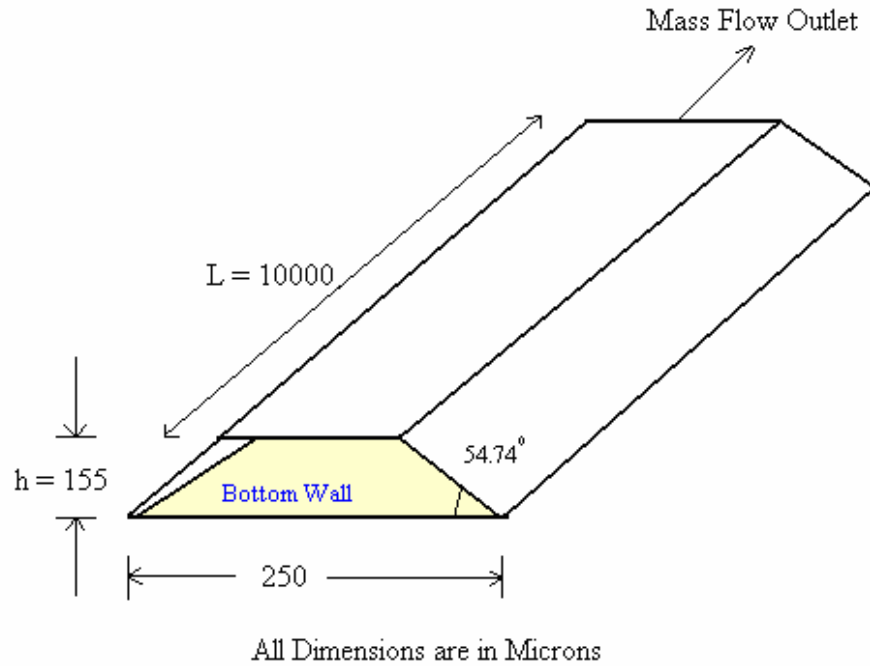


Figure 5: Trapezoidal microchannel with dimensions and outlet boundary conditions.

Each of the trapezoidal microchannels had a length of 1 cm as shown in Fig. 5. Only half the length of the microchannel was modeled due to symmetry of vapor flow existing in both the ends.

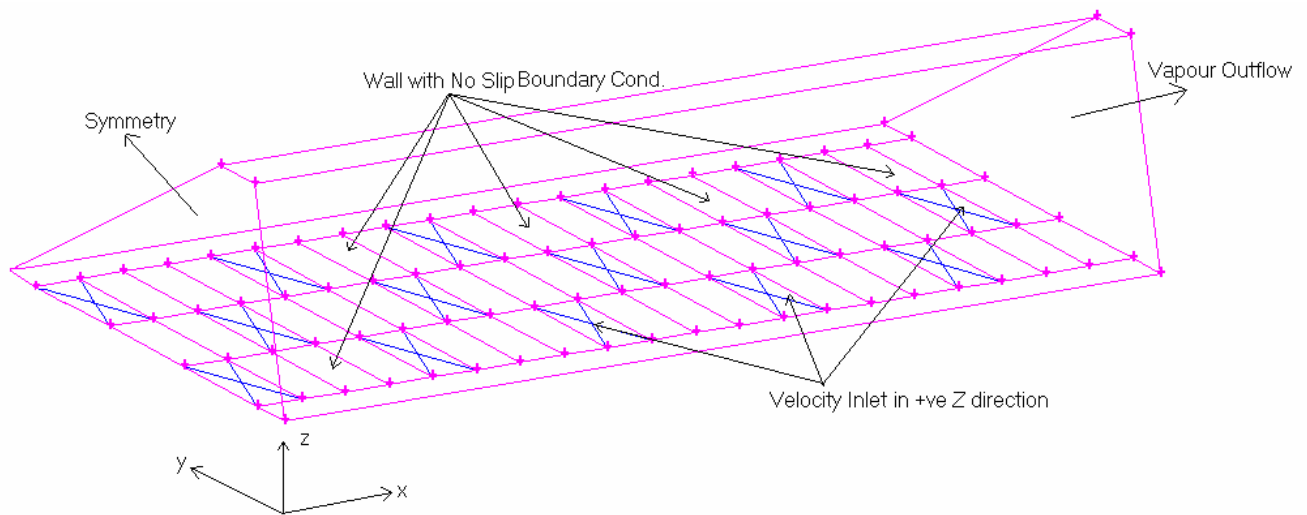


Figure 6: (a) Geometry of the trapezoidal microchannel showing boundary conditions and velocity inlet faces.

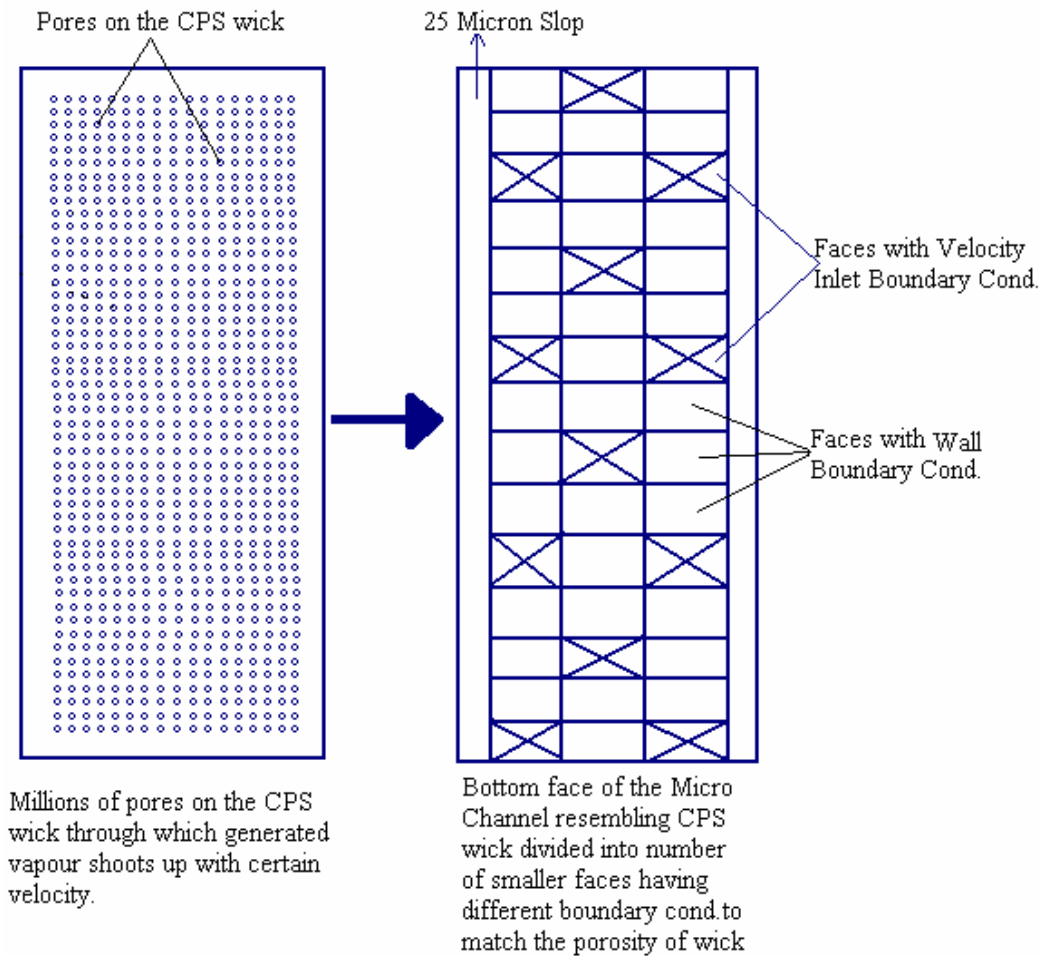


Figure 6: (b) Modeling of the bottom face of the trapezoidal microchannel resembling CPS wick in GAMBIT 2.1 replacing pores with square faces having velocity inlet boundary conditions to match the porosity.

The geometry of the trapezoidal microchannel was modeled in Gambit 2.1 as shown in Fig. 5. The CPS wick fabricated at the University of Cincinnati by the center for Micro Electronics and MEMS for the Micro-LHP demonstrator had a 5 micron pore diameter with a pitch of 10 microns. The pore patterning was done on the CPS wick to give a 25-micron slop as shown in the Fig. 6(a) to ensure that there were no pores covered by the rails. The porosity of the wick was determined to be 25%. Modeling of the porosity was attempted in the trapezoidal microchannel using GAMBIT 2.1 to determine the pressure drop. The bottom face of the trapezoidal microchannel resembling the CPS wick was divided into 60 faces as shown in the Fig. 6(a). Velocity inlet boundary condition depending on the mass flow rate was then applied to 15 faces as shown in the Fig. 6 (b) with cross marks thus maintaining the 25% porosity. This alternate arrangement of wall and velocity inlet boundary conditions closely simulated the flow of vapor over the CPS wick. In reality there are millions of such pores/faces on the wick making modeling complex and impossible.

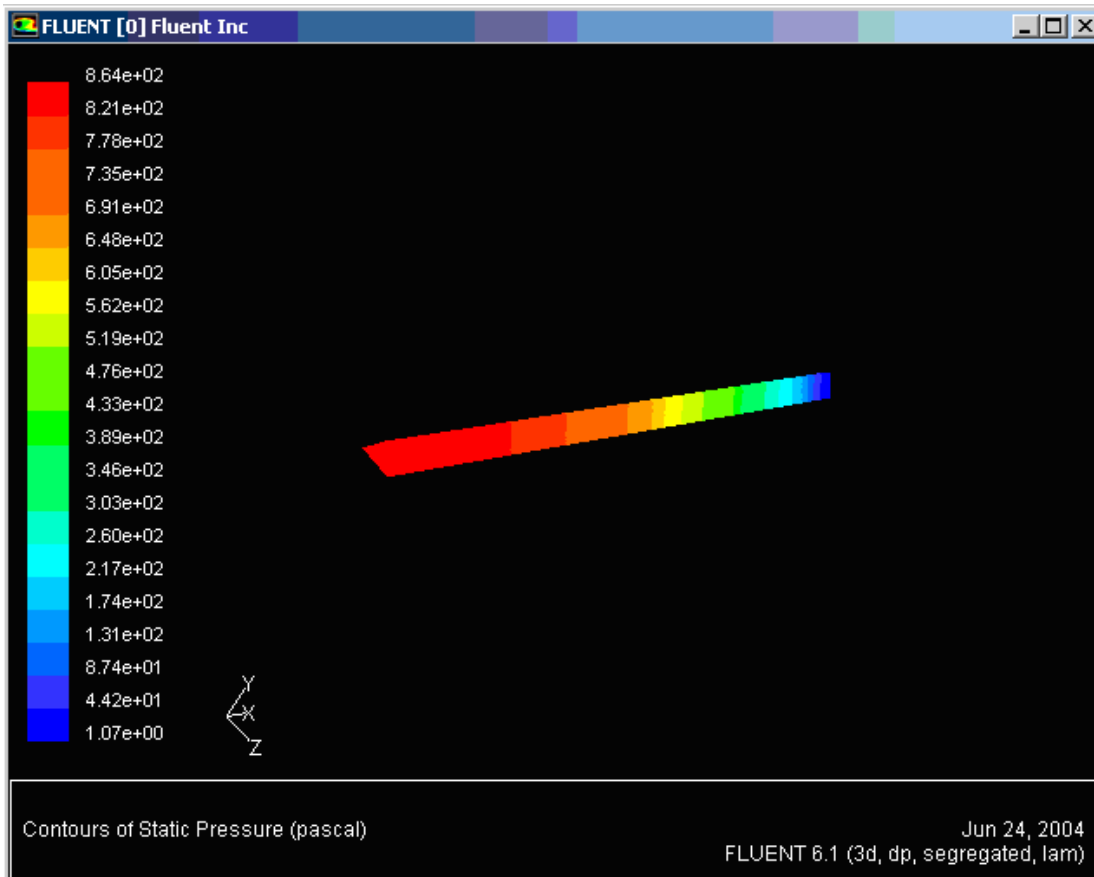


Figure 7: Contours of Pressure drop “865” Pa for power input of 25 W in the trapezoidal microchannel.

FLUENT 6.1 was used to determine the exact pressure drop in the trapezoidal microchannel. Uniform velocity inlet boundary condition with no slip was used for all inlet faces. Gauge pressure outside the vapor exit was taken as zero. The boundary layer was captured with very fine mesh near the wall regions for the greater accuracy of the results. The pressure drop in the microchannel was found to be 865 Pa for 25 W power as shown in the Fig. 7 above. This pressure drop was very less compared to the limiting burst through pressure.

Porosity of the CPS wick had a considerable effect on the pressure drop in the microchannel.

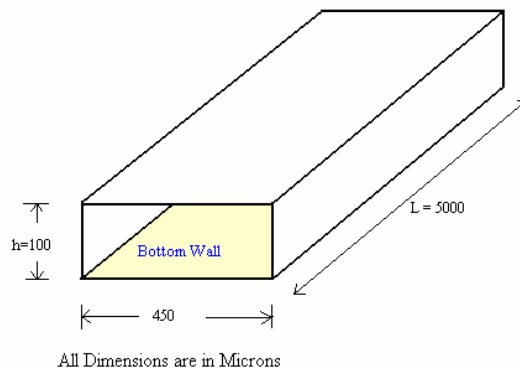


Figure 8: Rectangular microchannel with dimensions.

The geometry of the rectangular slot top cap design was numerically modeled as shown in the Fig. 8 to study the effect of porosity on the pressure drop. The bottom face resembling the CPS wick was divided into 60 faces and had a 30 microns slot for pore patterning. The porosity in the wick was varied by varying the number of faces with velocity inlet boundary conditions in the bottom face of the microchannel. The pressure drop was numerically calculated using FLUENT 6.1. Uniform velocity inlet boundary condition with no slip was used for all inlet faces. Gauge pressure outside the vapor exit was taken as zero.

| Porosity % | Pressure Drop (Pa) |
|------------|--------------------|
| 21.67      | 611                |
| 30.31      | 581                |
| 43.33      | 573                |

Table 2: Table showing pressure drop with respect to porosity for 25 W power input.

The pressure drop for different porosities were as shown in the table [2] for the power input of 25 Watts. It was seen that higher the porosity, lower was the pressure drop. This was due to the fact that the effective surface area of the silicon on the CPS wick decreases with increase in the porosity and hence vapor flow experiences less shear stress. In trapezoidal slot top cap the vapor generated exit from the reservoirs provided at both ends causing additional pressure drop as shown in Fig. 9.

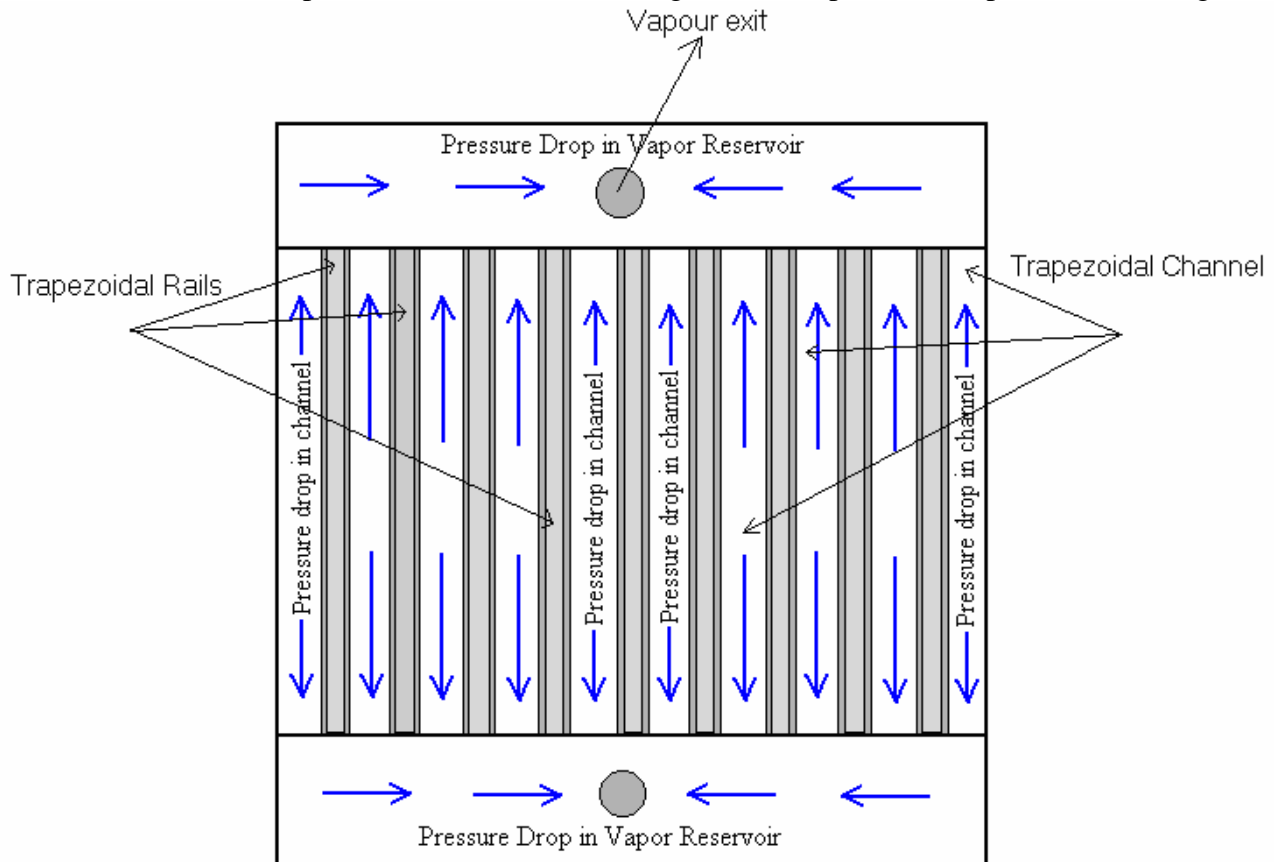


Figure 9: Top view of trapezoidal slot top cap showing vapor flow and types of pressure drop.

The vapor reservoir was etched using KOH etching from a 650 microns thick silicon wafer. The width of the reservoir was fixed at 2000 microns. The geometry of the reservoir was created in

GAMBIT 2.1 and modeled for pressure drop using FLUENT 6.1 to determine the best possible height. The height of the reservoir was varied from 1414.5-155 microns. Only half the geometry of the vapor reservoir was modeled due to symmetry.

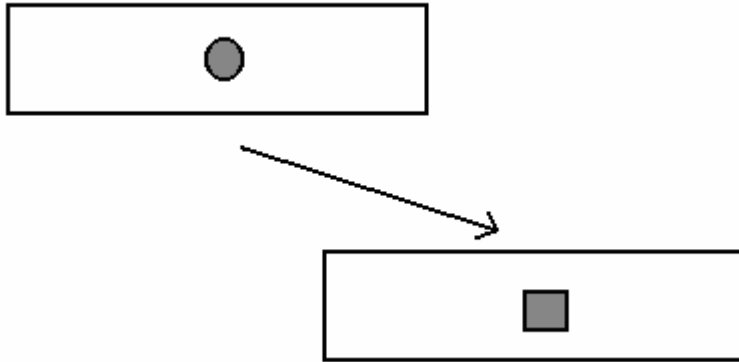


Figure 10: Approximation of circular vapor exit to square exit.

For easier meshing the circular vapor exit was approximated as square vapor exit as shown in the Fig. 10.

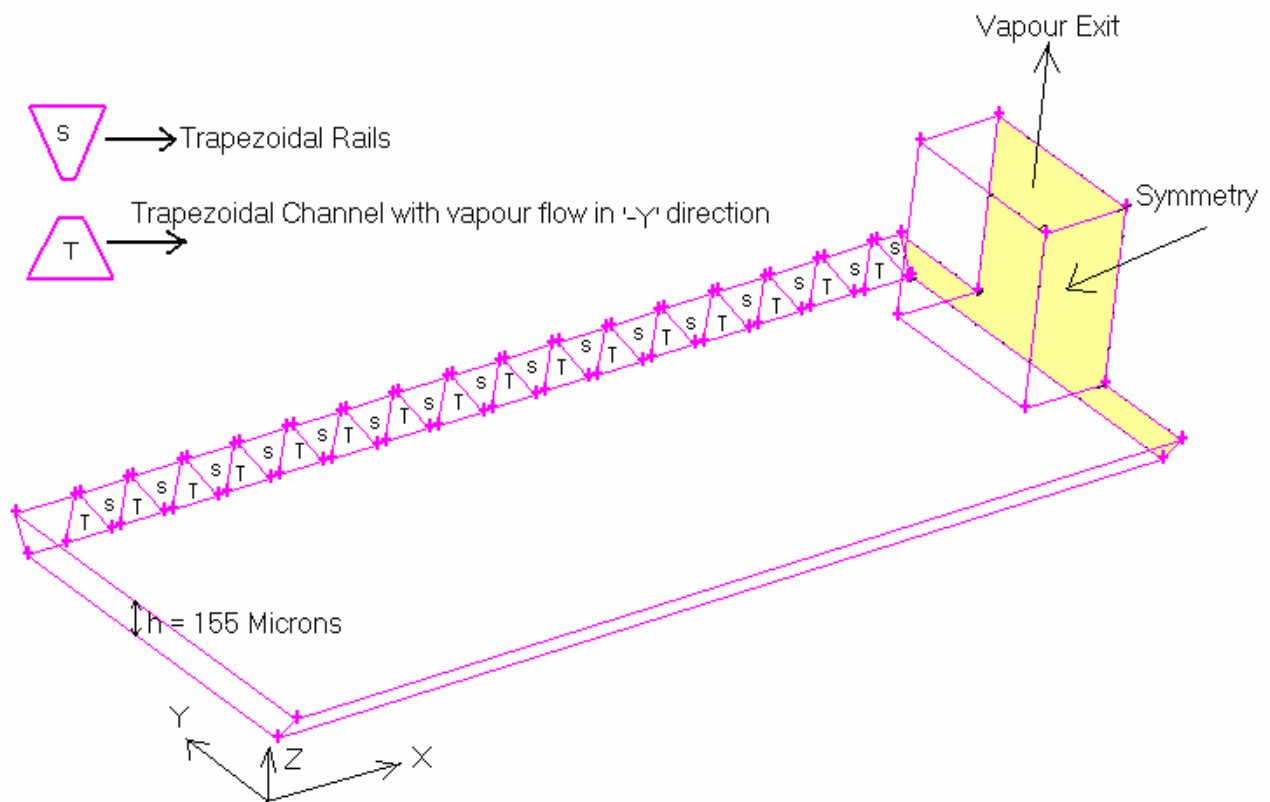


Figure11: Geometry of the vapor reservoir for height 155 microns showing boundary conditions.

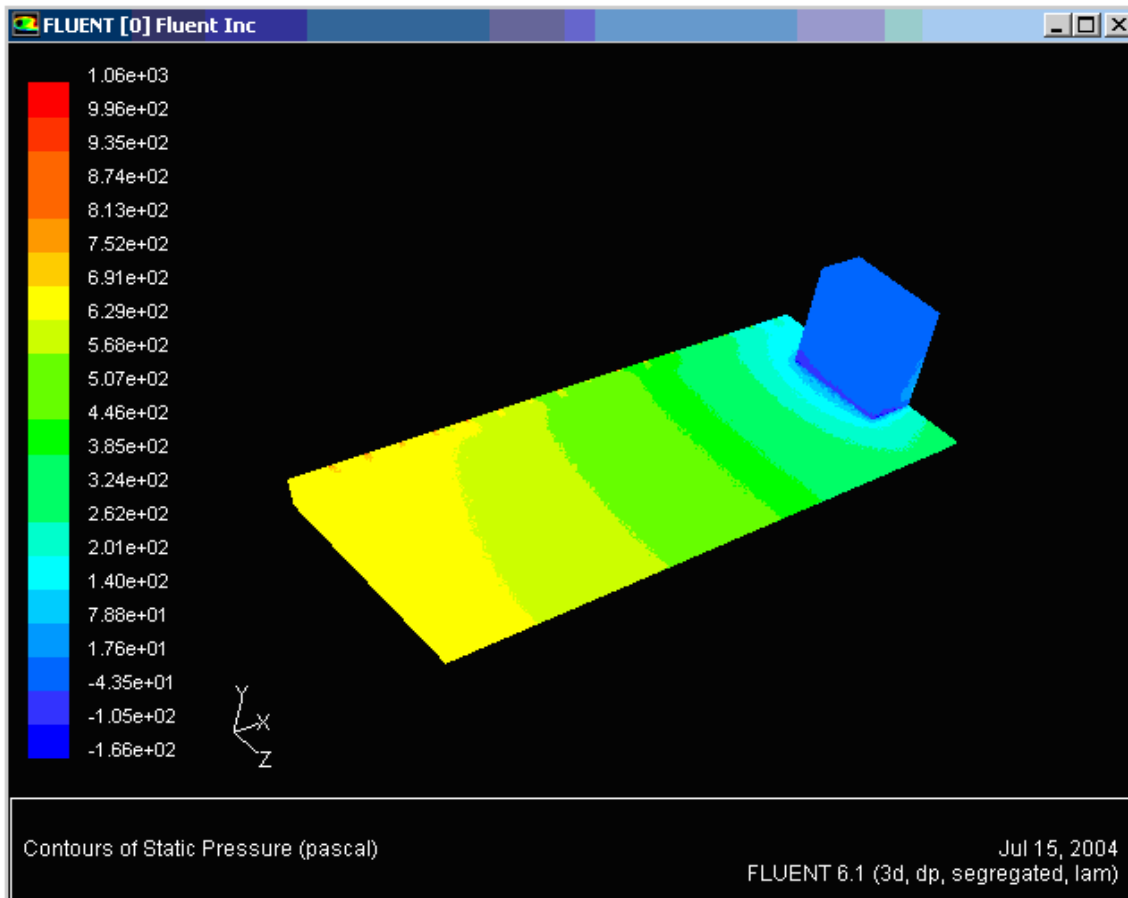


Figure 12: Contours of pressure drop “1226” Pa for 25W power in the vapor reservoir for height of 155 microns.

Fig. 11 shows the GAMBIT geometry of the modeled vapor reservoir with height of 155 microns. The small trapezoids on one face of the vapor reservoir were the entry of vapor in the reservoir from trapezoidal microchannel. Here the height of the reservoir was same as the height of the trapezoidal microchannel. Fig 12 shows the contours of pressure drop (1226 Pa) determined by the FLUENT 6.1 in the vapor reservoir for the height of 155 microns. Uniform velocity inlet boundary condition with no slip was used for all inlet faces. Gauge pressure outside the vapor exit was taken as zero. The pressure drop was higher than that of the pressure drop in the microchannel shown in Fig. 7. Total pressure drop in the top cap is the sum of pressure drop in microchannel vapor reservoir and found to be 2091 Pa.

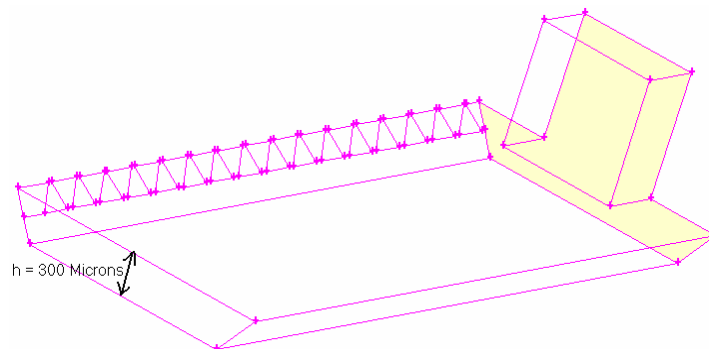


Figure 13: Geometry of the vapor reservoir for height of 300 microns.

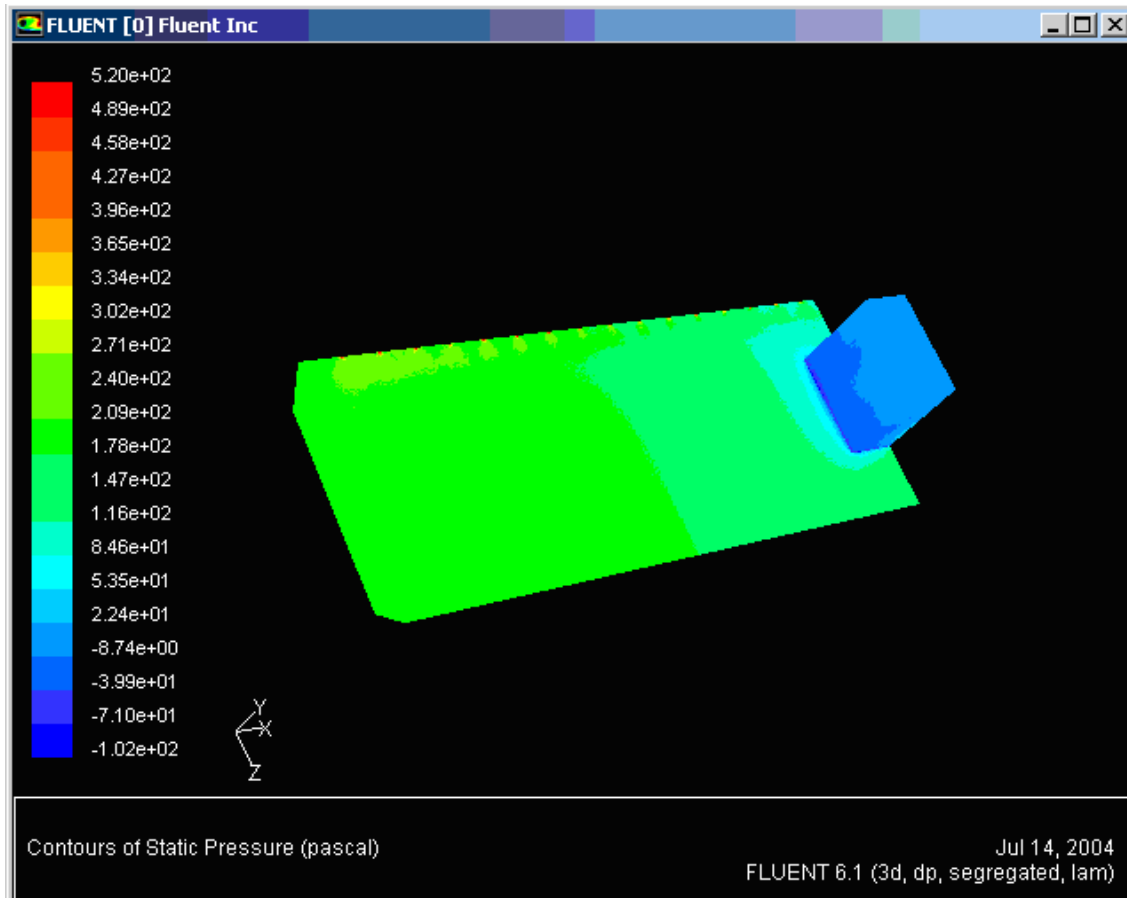


Figure 14: Contours of pressure drop “622” Pa for 25W power in the vapor reservoir for height of 300 microns.

Fig. 13 shows the GAMBIT geometry of the modeled vapor reservoir with height of 300 microns. Here the height of reservoir was higher than that of trapezoidal micro channel. Fig. 14 shows the pressure drop (622 Pa) determined by the FLUENT in the vapor reservoir for the height of 300 microns. This pressure drop is lower than that of the pressure drop in the microchannel shown in Fig. 7. Total pressure drop in the top cap is the sum of pressure drop in microchannel and vapor reservoir and found to be 1487 Pa.

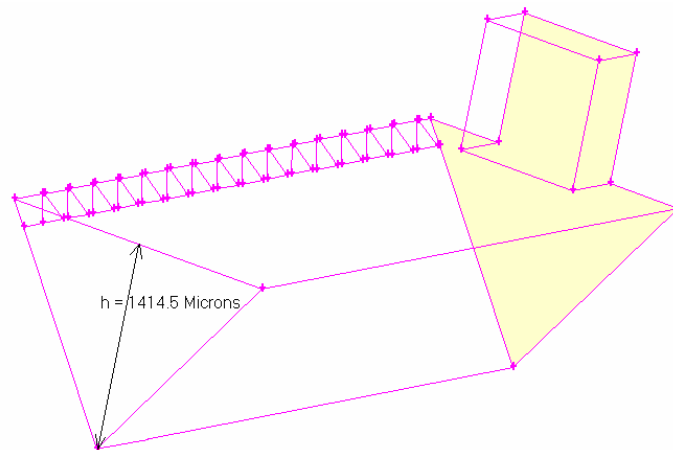


Figure 15: Geometry of the vapor reservoir for height 1414.5 microns.

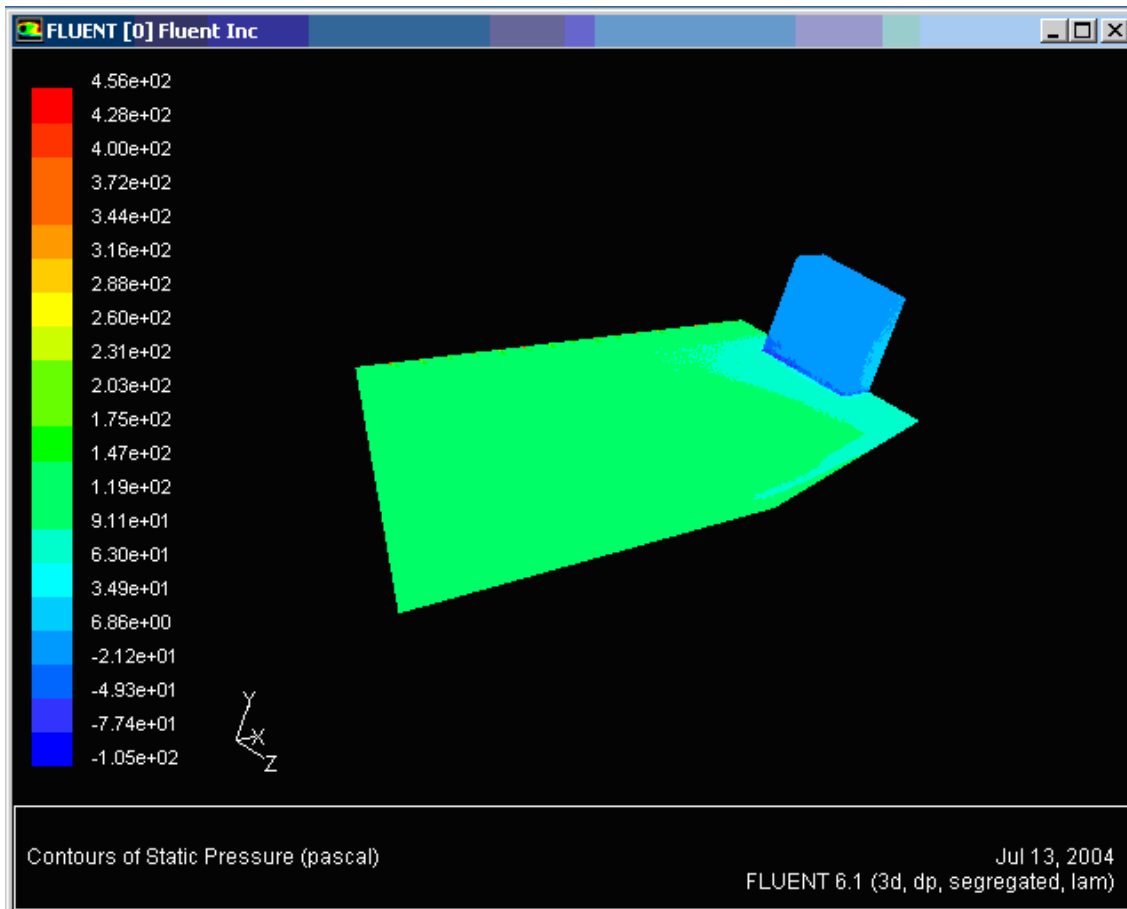


Figure 16: Contours of pressure drop “561” Pa for 25W power in the vapor reservoir for height of 1414.5 microns.

Fig. 15 shows the GAMBIT geometry of the modeled vapor reservoir with height of 1414.5 microns. Here the height of reservoir was higher than that of trapezoidal microchannel. This height is the limiting height of the vapor reservoir by KOH etching technique for a given width of 2000 microns. Fig. 16 shows the pressure drop (561 Pa) determined by the FLUENT 6.1 in the vapor reservoir for the height of 1414.5 microns. This pressure drop is lower than that of the pressure drop in the microchannel shown in Fig.7. Total pressure drop in the top cap is the sum of pressure drop in microchannel and vapor reservoir and found to be 1426 Pa.

Though the pressure drop was very low comparatively for the height of 1414.5 microns but is impracticable as the height of the silicon wafer was only 650 microns. Thus the vapor reservoir with height of 300 microns will be fabricated as it was chosen to be the best from both pressure drop and fabrication point of view.

### Temperature Drop

So far the design of the trapezoidal slot top cap was optimized from pressure drop point of view. The trapezoidal slot top cap was analyzed for temperature drop in the trapezoidal rails using the commercially available finite element software ANSYS 6.1 with the boundary conditions as shown in the Fig. 17.

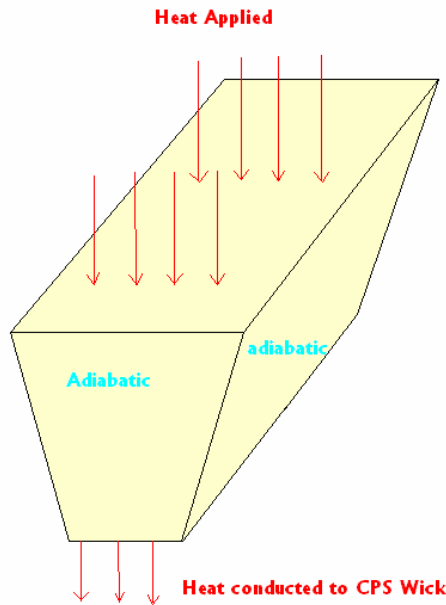


Figure 17: Thermal Boundary conditions applied on the trapezoidal rail.

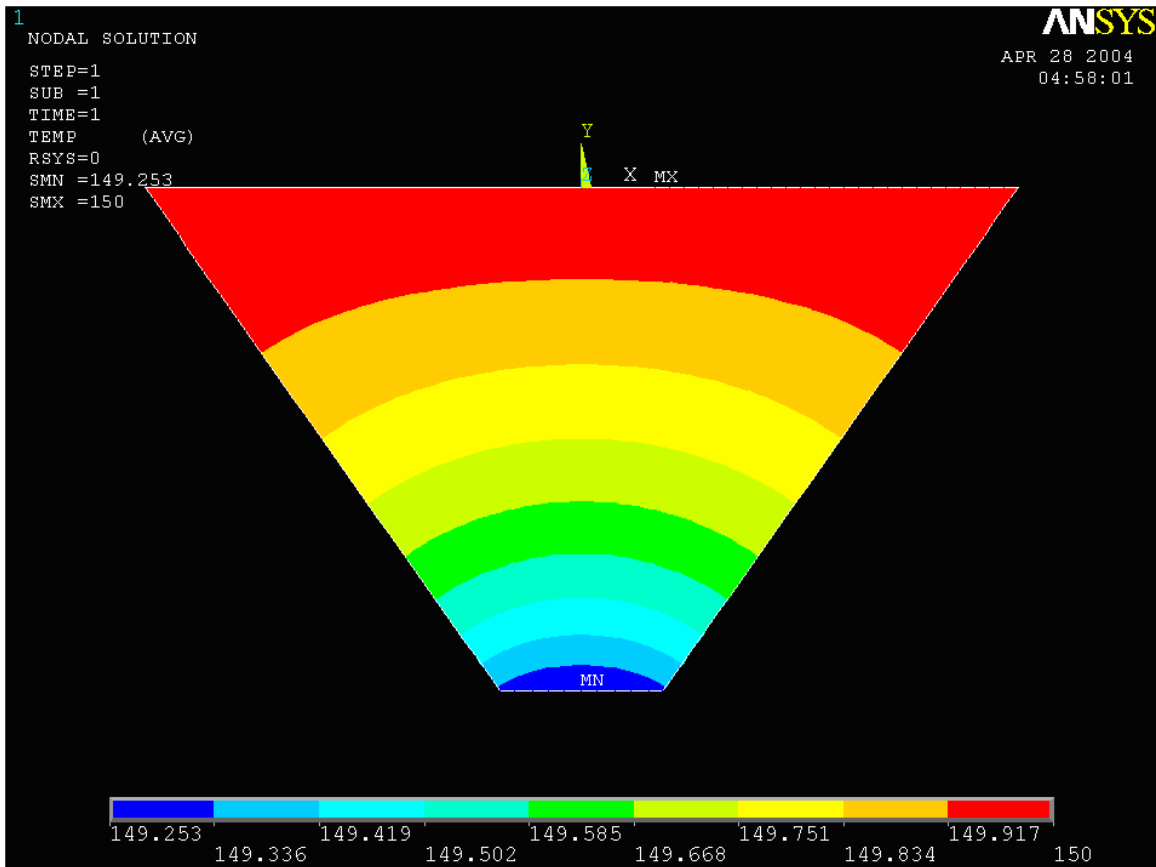


Figure 18: Contours of temperature drop of “0.75<sup>0</sup>” C in the rail for 25 W power.

Fig. 18 shows the temperature drop in the trapezoidal rail for the power input of 25W. This temperature drop of 0.75°C in the trapezoidal conduction pathway was very less compared to the temperature drop without conduction pathway which was of order of 39°C.

### Trapezoidal Mesas Top Cap Design

The optimal geometry of the trapezoidal mesas top cap given by Praveen et al [12] was shown in Fig. 19.

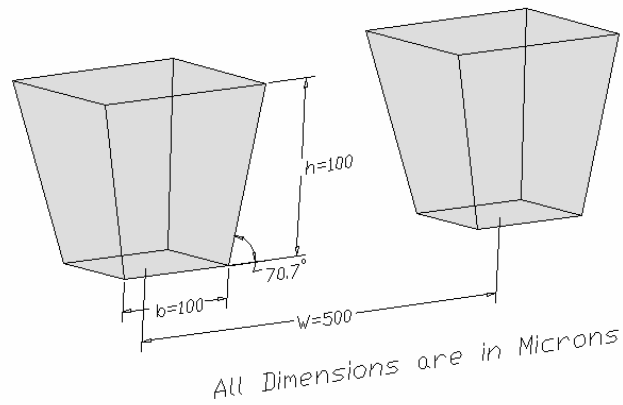


Figure 19: Optimal geometry of the trapezoidal mesas top cap.

Trapezoidal mesas conduction pathways were etched from a 650 microns silicon wafer with an etching angle of  $70.4^\circ$ . The post bottom width ‘b’ of the mesa was 100 microns. The height of mesa ‘h’ was 100 microns. The center to center spacing between the mesas was 500 microns and hence there were  $20 \times 20 = 400$  such mesas in 1cm X 1cm Silicon wafer. Top cap with trapezoidal mesas physically resembles 1 cm X 1 cm X 100 micron vapor reservoir having 400 trapezoidal columns/pillars with one hole in the center for vapor exit. This paper analyses and presents the pressure drop of such 1 cm \*1cm\*100 micron vapor reservoir with and without trapezoidal columns conduction pathways. The circular hole for the vapor exit was approximated as a square hole for easier meshing as shown in Fig. 20.

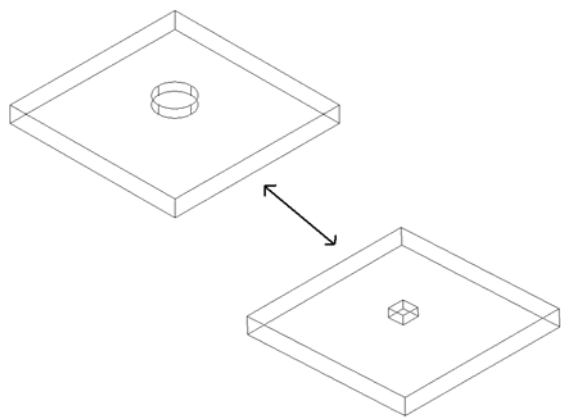


Figure 20: Approximation of circular vapor exit to square exit for easier meshing.

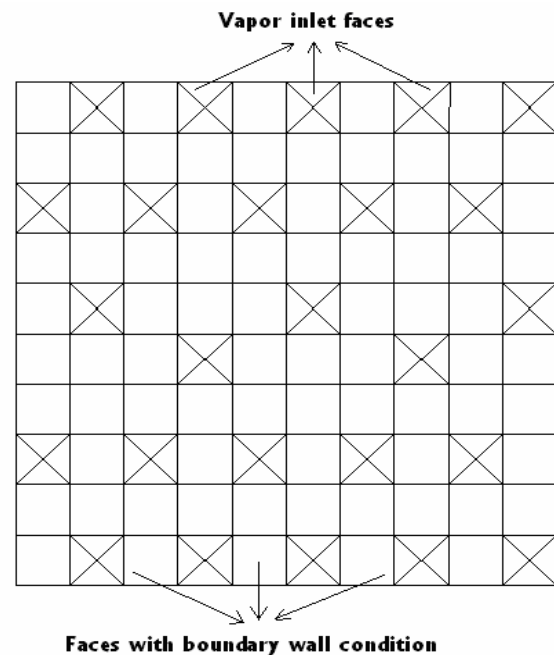


Figure 21: Bottom face/ wall of the vapor reservoir showing boundary conditions.

The symmetric geometry of the vapor reservoir with and without trapezoidal mesas was modeled in GAMBIT 2.1 assuming the porosity of the CPS wick as 25%. The bottom face of the vapor reservoir resembling CPS wick was divided into 100 smaller faces as shown in the Fig. 21 . Vapor inlet (depending on mass flow rate ) boundary condition was applied to 25 such faces as shown in the Fig 21.with crossed marks to maintain 25% porosity.

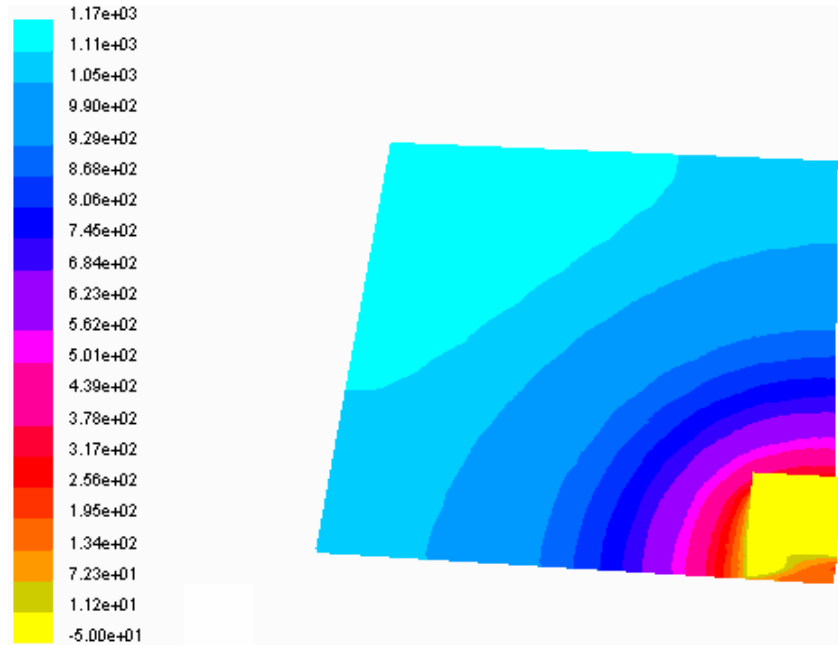


Figure 22: (a) Top view of contour of pressure drop “1220” Pa for 25 W heat input in the vapor reservoir without conduction pathways.

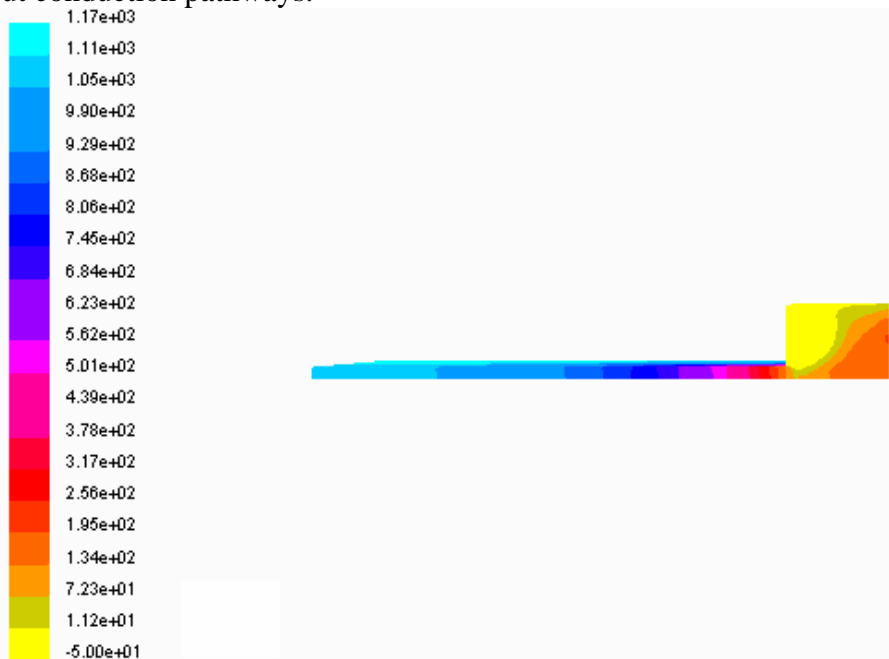


Figure 22: (b) Side view of contour of pressure drop “1220” Pa for 25 W heat input in the vapor reservoir without conduction pathways.

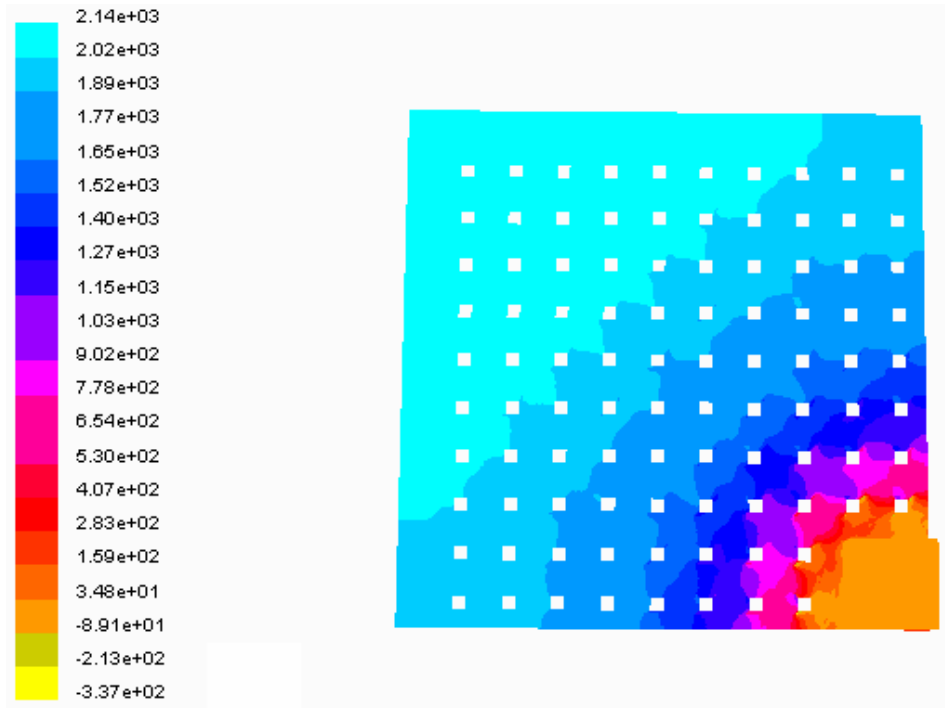


Figure 23: (a) Top view of contour of pressure drop “2477” Pa for 25 W heat input in the vapor reservoir with trapezoidal mesas conduction pathways

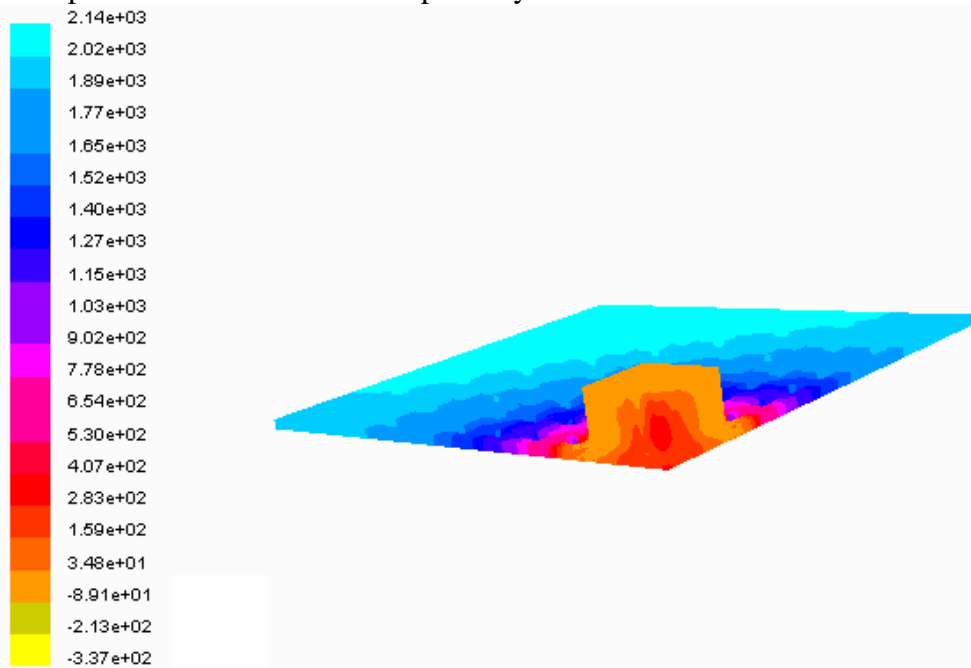


Figure 23: (b) Side view of contour of pressure drop “2477” Pa for 25 W heat input in the vapor reservoir with trapezoidal mesas conduction pathways

FLUENT 6.1 was used to determine the pressure drop in the optimal vapor reservoir. Uniform velocity inlet boundary condition with no slip was used for all inlet faces. Gauge pressure outside the vapor exit was taken as zero. The mesh density was very high near the wall regions to capture boundary layer for greater accuracy of the results. The values of the pressure drop in the vapor reservoir with and without trapezoidal mesas were as shown in the Fig 22, 23. It could be seen that pressure drop in the vapor reservoir without trapezoidal mesas was 1220 Pa for 25 W power. This is

much lower than the pressure drop with trapezoidal mesas which had the pressure drop of 2477 Pa. The trapezoidal mesas columns increase the pressure drop of the vapor flow in the reservoir by generating vorticities and thereby adding viscous losses. But the pressure drop of 2477 Pa with trapezoidal mesas was within the optimal limits given by Praveen et al [12].

### Temperature drop

Optimal geometry of the trapezoidal mesas was analyzed for temperature drop using commercially available finite element software ANSYS 6.1 with the boundary conditions as shown in the Fig .24.

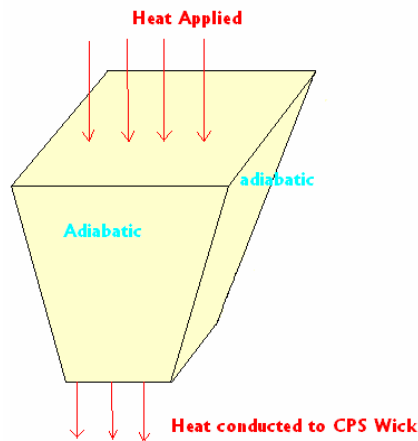


Figure 24: Thermal boundary conditions applied on the trapezoidal mesas.

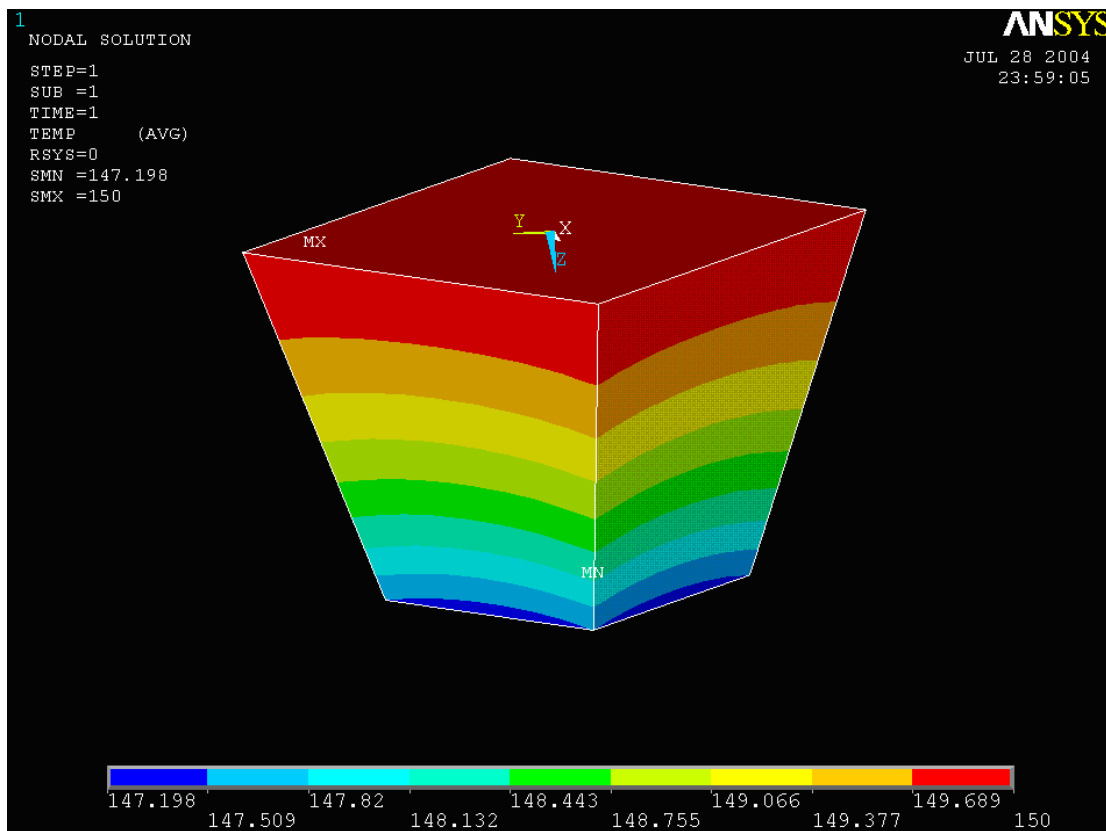


Figure 25: Contours of temperature drop “2.8<sup>0</sup>” C in the trapezoidal mesas for 25 W power.

Fig. 25 shows the temperature drop in the trapezoidal mesas for the power input of 25W. This temperature drop of 2.8<sup>0</sup>C in the trapezoidal mesa conduction pathway was very less compared to the temperature drop without conduction pathway which was of order of 39<sup>0</sup>C. It was clearly seen that the presence of trapezoidal mesas increases the pressure drop by about 100% but temperature drop was decreased tremendously.

## CONCLUSION

The problem of non uniform conduction of heat from the source to the CPS wick was identified and overcome by the provision of conduction pathways. Five different feasible competitive designs of the top cap with conduction pathways were considered and studied. Of the five designs, trapezoidal slot and trapezoidal mesas top cap were relatively easy to fabricate with the available MEMS fabrication technology. The conduction pathways reduced the temperature drop in the top cap but simultaneously increased the pressure drop of the vapor. Geometries of the trapezoidal slot and trapezoidal mesas top cap were chosen from the optimal solutions for perfect contact based on the approximate analysis of pressure and temperature drop. The exact pressure drop and temperature drop in the chosen geometries of trapezoidal slot and trapezoidal mesas were found to be little higher than approximate analysis but were within the optimal limit. These geometries of the trapezoidal slot and Trapezoidal mesas were considered to be optimal and are ready to be fabricated. Porosity had considerable effect on the pressure drop. It was found that higher the porosity, lower was the pressure drop.

## ACKNOWLEDGEMENTS

This research was sponsored by the NASA John H. Glenn Research Center at Lewis Field (GRC) under contract number C-80063-A and C-80075-A. A special thanks to Kenneth Mellott and Jake Kim for their continued support of and input to the project. Research team would also like to thank the following people Praveen Medis, Srinivas Parimi, Ahmed Shuja, Debra Cytrynowicz, Junwoo Suh , Priyanka Ponugoti and Monika Sharma at University of Cincinnati for their assistance with various activities of the project.

## REFERENCES:

- [1]A. V. Alexseev, "Micro Loop Heat Pipe Evaporator Coherent Pore Structures", Master thesis, Texas A&M University, 2003.
- [2] Hamdan Mohammad Omar, " Loop Heat Pipe (LHP) Modeling And Development By Utilizing Coherent Porous Silicon (CPS) Wicks", PhD Thesis, University Of Cincinnati, Mechanical Engineering, 2003.
- [3] Holke A., Henderson T., Gerner F., and Kazamierczak M., "Analysis of Heat Transfer Capacity of a Micro-machined Loop Heat Pipe", Asme Journal Of Heat Transfer, submitted for publication, 1999.
- [4] Chandratilleke C., Hatakeyama H., and Nakagome H., "Development of Cryogenic Loop Heat Pipes", Cryogenics, Vol. 38, No. 3, pp. 263-269, 1998.
- [5] Nikitkin M., and Cullimore B., "CPL and LHP Technologies: What are the Differences, What are the Similarities?", SAE Paper 981587, 1998.
- [6] Swanson L., and Herdt G., "Model of the evaporating meniscus in capillary tube", Asme Journal Of Heat Transfer, Vol. 114, pp. 434-440, 1992.
- [7] Kaya T., and Hoang T., "Mathematical Modeling of Loop Heat Pipes and Experimental Validation", J. of Thermo physics and Heat Transfer, Vol. 13, No. 3, pp.

314-320, 1999.

[8] Kamotani Y., “Thermocapillary Flow Under Microgravity – Experimental Results”, *Adv Space Res.*, Vol. 24, No. 10, pp 1357-1366, 1999.

[9] Tarik K., and Jentung Ku., “Thermal Operational Characteristics of a small Loop Heat Pipe”, *Journal of Thermo physics and Heat Transfer*, Vol. 17, pp 464-470, 2003.

[10] Figus C., Le Bray Y., Bories S., and Part M., “Heat and Mass Transfer with Phase Change in a Porous Structure Partially Heated: Continuum Model and Pore Network Simulations”, *Int. J. of Heat and Mass Transfer*, Vol. 42, pp. 2557-2569, 1999.

[11] Thiago D., and Roger R.R., “Analysis of the Thermal Performance of a Loop Heat Pipe”, *ASME International Mechanical Engineering Congress*, 2003.

[12] Praveen A., “Competitive Optimal Top Cap Designs of Micro Loop Heat Pipe”, Master thesis, University of Cincinnati, Mechanical Engineering, 2005.

[13] Praveen A., Gerner F.M., and Henderson H.T., “Competitive Designs of Evaporator Top Cap of the Micro Loop Heat Pipe”, *ASME International Mechanical Engineering Congress*, 2004.